# Eliminating Angular Dispersion in Microcavity by Employing Metamaterials With Hyperbolic Dispersion as Reflectors

Xu-Lin Zhang, Jun-Feng Song, Jing Feng, and Hong-Bo Sun, *Member, IEEE*

*Abstract*—Microcavity typically exhibits a blue shift of the resonance with the angle increasing, which may bring disadvantages in related applications. Herein, we propose a design concept of eliminating the angular dispersion in microcavity by employing metamaterials with hyperbolic dispersion as reflectors. By exploiting optimal constitutive parameters of the metamaterials, the reflection phase from the cavity upon both metamaterial reflectors increases drastically with the incident angle, and can nearly compensate the decrement of the phase accumulation inside the cavity for each angle. A microcavity without angular dispersion is therefore established, in which the metamaterials may be realized by employing metal–dielectric multilayered structures in practice.

*Index Terms*—Microcavity, angular dispersion, metamaterials with hyperbolic dispersion.

## I. Introduction

RESONANT microcavity configurations, such as the metal/dielectric/metal structures, have been explored extensively for applications of sensors [1], lasers [2], optical filters [3], light-emitting devices [4]–[7], and solar cells [8]. On resonance, microcavity devices can exhibit improved performance due to the enhanced light-matter interaction in the cavity. For instance, enhanced light absorption can be achieved in solar cells via the microcavity resonance [8]. However, the microcavity structures typically exhibit a blue shift of the resonant wavelength with the angle increasing, also called angular dispersion, which may bring disadvantages, such as in light-emitting devices that the emitting colors will change with the viewing angle varying [5], [6]. Similarly, the overall absorptivity will decrease drastically with the incident angle increasing in microcavity solar cells [8]. Therefore, lots of techniques have been proposed to overcome the angular dispersion, such as those by introducing conjugated polymer based

X.-L. Zhang, J. Feng, and H.-B. Sun are with the State Key Laboratory on Integrated Optoelectronics, College of Electronic Science and Engineering, Jilin University, Changchun 130023, China (e-mail: hbsun@jlu.edu.cn).

J.-F. Song is with the State Key Laboratory on Integrated Optoelectronics, College of Electronic Science and Engineering, Jilin University, Changchun 130023, China, and also with the Institute of Microelectronics, Agency for Science, Technology and Research, Singapore 117685 (e-mail: songjf@ime.a-star.edu.sg).

Color versions of one or more of the figures in this paper are available online at http://ieeexplore.ieee.org.

cavities [9], applying asymmetric Bragg mirrors [10], and using dispersive gratings [11]. However, the angular dispersion in these designs cannot be eliminated thoroughly but only suppressed to some extent.

Recently, metamaterials with hyperbolic dispersion have drawn more and more attentions due to their anomalous electromagnetic features. A lot of intriguing applications, such as cavities with anomalous scaling laws [12], invisibility cloaking [13], loss induced transmission [14], negative index photonic crystals [15], and tunable magnetic response [16], have been proposed by employing such metamaterials. Inspired by these progresses, microcavity without angular dispersion can be expected and is needed to be investigated if it is designed with metamaterials.

In this work, metamaterials with hyperbolic dispersion are applied as the reflectors of the microcavity. We find by choosing optimal constitutive parameters of the metamaterials, the reflection phase from the cavity upon the metamaterial reflectors can be designed to exhibit an anomalous rapid increment with the angle increasing. Such phase increment can, for each incident angle, nearly compensate the decrement of the phase accumulation inside the cavity. Therefore, a microcavity without angular dispersion can be established. The physical origin as well as the design principle is thoroughly investigated and discussed. We also demonstrate the possibility in realization of such microcavity by employing the realistic metal-dielectric multilayered structures as the metamaterial reflectors.

## II. Results and Discussions

### A. Design of Microcavity Without Angular Dispersion

We start from considering transverse-magnetic (TM) polarized plane wave incidence from air upon a conventional Ag (30 nm)/dielectric/Ag (100 nm) microcavity. The incident angle is defined by $\theta$, and the refractive index and thickness of the cavity are denoted as $n_c = 1.7$ and $d = 150$ nm. From the phase point of view, the microcavity resonance reads [17]:

$$\varphi_{sum} = \varphi_{up} + \varphi_{down} + \varphi_{cavity} = 2m\pi \tag{1}$$

where, as depicted in the inset of Fig. 2(a), $\varphi_{up}$ and $\varphi_{down}$ are reflection phases from cavity upon the reflectors, $\varphi_{cavity}$ is the one-round phase accumulation inside the cavity, and $m$ is an integer. The terms $\varphi_{up}$ and $\varphi_{down}$ can be calculated by the transfer matrix method [18], and $\varphi_{cavity}$ can be solved
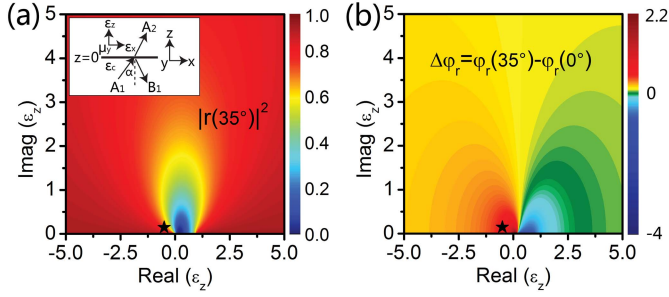
Fig. 1. Reflectivity $|r|^2$ for $\alpha = 35°$ (a) and reflection phase difference $\Delta\varphi_r$ between $\alpha = 35°$ and $\alpha = 0°$ (b) for TM waves from an isotropic cavity ($\varepsilon_c = 1.7^2$) upon anisotropic metamaterials ($\varepsilon_x = \varepsilon_{Ag}, \varepsilon_z, \mu_y = 1$) as a function of $\varepsilon_z$. The wavelength is chosen as 693 nm with $\varepsilon_{Ag} = -18.0 + 1.3j$. The black stars represent the region where both near-unity $|r|^2$ and positive large $\Delta\varphi_r$ exhibit.

directly by $\varphi_{cavity} = 2k_0d\sqrt{n_c^2 - \sin^2\theta}$, where $k_0$ ($=2\pi/\lambda$) is the wave vector in free space. In the calculations, the Ag permittivity $\varepsilon_{Ag}$ is extracted from the Rsoft package [19]. The phase variations as a function of wavelength for $\theta = 0°$ (solid lines) and $\theta = 80°$ (dashed lines) are shown in Fig. 2(a), where the intersections between the total phase $\varphi_{sum}$-line and $2\pi$-line correspond to the first-order resonant wavelengths. A blue shift of the resonance can be observed with increasing $\theta$, which can mainly be attributed to the decrease of $\varphi_{cavity}$, since $\varphi_{up}$ and $\varphi_{down}$ do not exhibit contributed distinctions for the two angles. The absorptivity spectrum, plotted in Fig. 2(d), also confirms the blue shift, and agrees well with the phase analysis.

Once the cavity parameters are determined, the variation trend of $\varphi_{cavity}$ cannot be avoided. Therefore, to eliminate the angular dispersion, one should find ways to change the features of $\varphi_{up}$ and $\varphi_{down}$. More specifically, a reflector, upon which the reflection phase increases drastically with the incident angle, needs to be designed. Our approach is to replace the conventional metal reflectors with anisotropic metamaterials. To find optimal constitutive parameters of the metamaterials, we study the reflection phase for TM waves from one isotropic cavity with relative permittivity $\varepsilon_c$ upon anisotropic metamaterials. The schematic is illustrated in the inset of Fig. 1(a), where $A_1$, $B_1$, and $A_2$ represent the amplitude of incident, reflected, and transmitted waves, and $\alpha$ is the incident angle. The anisotropy of the metamaterials is indicated by $\varepsilon_x$ and $\varepsilon_z$, and we simply set $\mu_y = 1$. The magnetic component $H_y$ can then be expressed as $A_1\exp(-j\kappa_1 z) + B_1\exp(j\kappa_1 z)$ in the isotropic cavity and $A_2\exp(-j\kappa_2 z)$ in the metamaterials, where we define $\kappa_1 = k_0\sqrt{\varepsilon_c - \sin^2\alpha}$ and $\kappa_2 = k_0\sqrt{\varepsilon_x(1 - \sin^2\alpha/\varepsilon_z)}$. By applying the relationship $E_x = \dfrac{-j}{k_0\varepsilon_x}\dfrac{\partial H_y}{\partial z}$ as well as the continuity of $E_x$ and $H_y$ at the interface ($z = 0$) [17], we have $A_1 + B_1 = A_2$ and $(A_1 - B_1)\kappa_1/\varepsilon_c = A_2\kappa_2/\varepsilon_x$. Then we obtain the expression of the reflection coefficient:

$$r = \frac{B_1}{A_1} = \left(\frac{\kappa_1}{\varepsilon_c} - \frac{\kappa_2}{\varepsilon_x}\right)\bigg/\left(\frac{\kappa_1}{\varepsilon_c} + \frac{\kappa_2}{\varepsilon_x}\right) \qquad (2)$$

As for normal incidence, the metamaterials can be treated as isotropic media with permittivity $\varepsilon_x$, we set $\varepsilon_x = \varepsilon_{Ag}$ in all

this work to guarantee the metamaterials to act as reflectors. The reflectivity $|r|^2$ for $\alpha = 35°$ as well as the reflection phase difference $\Delta\varphi_r$ between $\alpha = 35°$ and $\alpha = 0°$ are calculated based on (2) and shown in Fig. 1(a) and (b) as a function of $\varepsilon_z$, respectively. The wavelength is chosen as 693 nm, the resonance in Fig. 2(a), with $\varepsilon_{Ag} = -18.0 + 1.3j$. We still choose $\varepsilon_c = 1.7^2$, and the transverse wave vector at $\alpha = 35°$ in such a cavity is equal to that at $\theta = 80°$ in air. Apparently, we need find a region where both near-unity $|r|^2$ and positive $\Delta\varphi_r$ as large as possible exhibit. Such region indeed exists and is located around the negative real axis as marked by the black star. Besides, the closer to the origin point, the larger positive $\Delta\varphi_r$ exhibits. Before applying this exotic feature, we demonstrate its physical origin. By considering $\varepsilon_z$ as a negative real number and using an approximation that $Re(n_{Ag}) \ll Im(n_{Ag})$ at optical frequencies, where $n_{Ag} = \sqrt{\varepsilon_{Ag}}$, the reflection coefficient can be derived as:

$$r(\alpha) \approx \frac{\sqrt{\varepsilon_c - \sin^2\alpha}/\varepsilon_c + j\sqrt{1 + \sin^2\alpha/|\varepsilon_z|}/Im(n_{Ag})}{\sqrt{\varepsilon_c - \sin^2\alpha}/\varepsilon_c - j\sqrt{1 + \sin^2\alpha/|\varepsilon_z|}/Im(n_{Ag})} \qquad (3)$$

The reflection phase then reads:

$$\varphi_r(\alpha) \approx 2\arctan\left(\frac{\varepsilon_c\sqrt{1 + \sin^2\alpha/|\varepsilon_z|}}{Im(n_{Ag})\sqrt{\varepsilon_c - \sin^2\alpha}}\right) \qquad (4)$$

We conclude from (3) and (4) that the reflectivity $|r|^2$ will be near-unity and $\varphi_r(\alpha)$ will increase with $\alpha$. Moreover, the smaller $|\varepsilon_z|$ is, the larger slope $\varphi_r(\alpha)$ exhibits. Therefore, by choosing $\varepsilon_z$ around the negative real axis as well as the original point, the metamaterials can be used as reflectors whose reflection phase increases rapidly with the incident angle. As such metamaterials exhibit a hyperbolic dispersion [12], [14], we simply call them as hyperbolic metamaterials in this work.

Microcavity without angular dispersion can then be expected by employing these metamaterials as reflectors. We reconsider the structure depicted in the inset of Fig. 2(a). This time the constitutive parameters of the metamaterials are chosen as $\varepsilon_x = \varepsilon_{Ag}$ and $\varepsilon_z = -0.77$. The phase variation and absorptivity spectrum are plotted in Fig. 2(b) and (e), respectively. Compared with the phase results at $\theta = 0°$, considerable phase increment can be provided by $\varphi_{up}$ and $\varphi_{down}$ at $\theta = 80°$. Such phase increment could nearly compensate the phase decrement by $\varphi_{cavity}$, resulting in a nearly invariable $\varphi_{sum}$ as well as the resonant wavelength. Interestingly, when $|\varepsilon_z|$ is further decreased to be $\varepsilon_z = -0.3$, as plotted in Fig. 2(c) and (f), even excess phase compensations can be provided by $\varphi_{up}$ and $\varphi_{down}$, inducing an anomalous red shift of the resonance. In the inset of Fig. 2(e), we add a calculation of the iso-frequency contour of the metamaterials at the resonant wavelength of ~693 nm, where $k_x$ and $k_z$ represent the x- and z-direction wave vectors in the metamaterials, respectively. The results verify the hyperbolic dispersion of the metamaterials.

In Fig. 2(a)–(f), we have investigated the microcavity with three sets of constitutive parameters but only at two incident angles. To gain a comprehensive understanding of the microcavity features at all angles, we fix the wavelength at 693 nm,
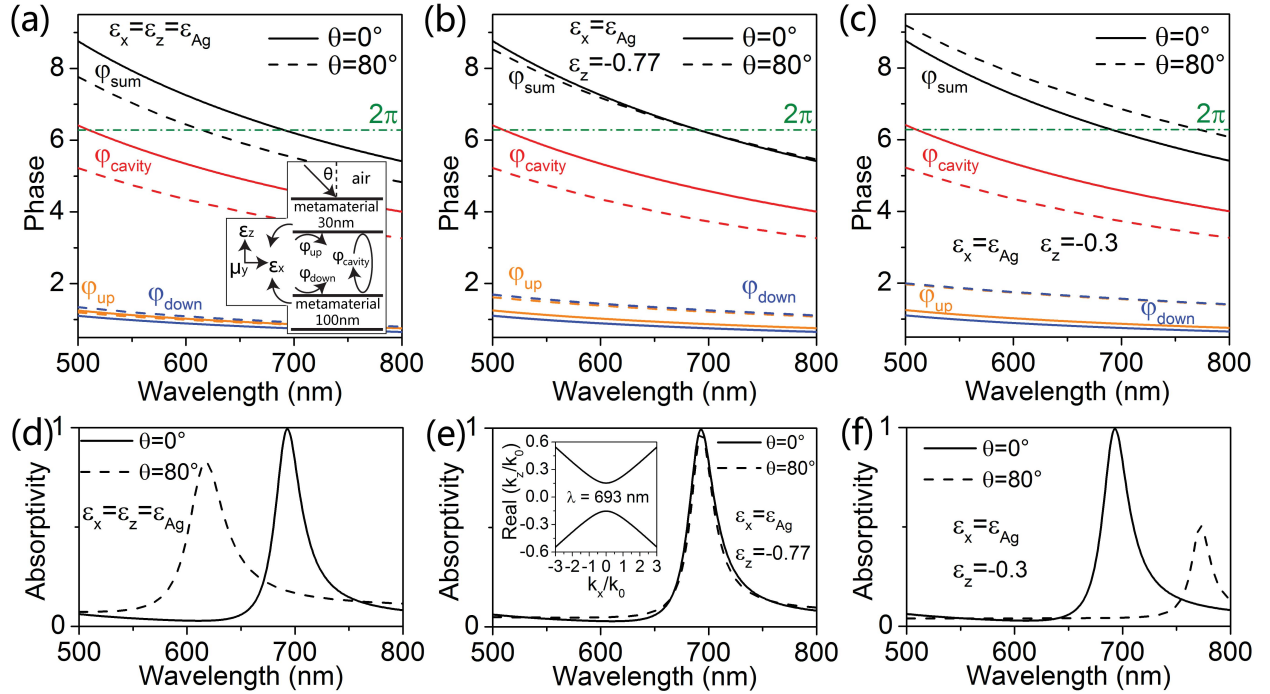
Fig. 2. Phase variations in the metamaterial (30 nm)/dielectric/metamaterial (100 nm) microcavity as a function of wavelength with constitutive parameters of $\varepsilon_z = \varepsilon_{Ag}$ (a), $\varepsilon_z = -0.77$ (b), and $\varepsilon_z = -0.3$ (c). The corresponding TM-polarized absorptivity spectra are plotted in (d), (e), and (f), respectively. In all figures, we choose $\varepsilon_x = \varepsilon_{Ag}$ and cavity parameters of $n_c = 1.7$ and $d = 150$ nm. The solid and dashed lines correspond to the results for $\theta = 0°$ and $\theta = 80°$, respectively. Inset of (e) shows the hyperbolic dispersion of the metamaterials.
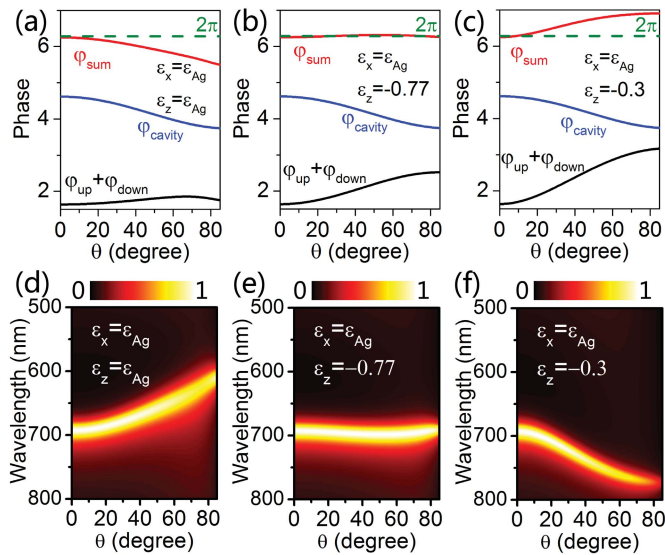


Fig. 3. Phase variations at wavelength of 693 nm as a function of incident angle (a)–(c). Absorptivity dispersions of the microcavity for TM-polarized incidence as a function of wavelength and incident angle (d)–(f). The microcavity parameters are chosen as $n_c = 1.7$ and $d = 150$ nm, and the constitutive parameters of the metamaterials are indicated in each figure.

the resonance at normal incidence, to calculate the phase variations as a function of the incident angle. The results are plotted in Fig. 3(a)–(c) for the same three sets of constitutive parameters, and the corresponding absorptivity dispersions are illustrated in Fig. 3(d)–(f), respectively. It is noted from

Fig. 3(b) that by employing hyperbolic metamaterials with constitutive parameters optimally chosen, the variation trend of $\varphi_{cavity}$ can nearly be compensated by $\varphi_{up} + \varphi_{down}$ in each angle, since the $\varphi_{sum}$-line and the $2\pi$-line almost coincide with each other. A microcavity without angular dispersion is therefore established, which can also be verified by the absorptivity dispersion shown in Fig. 3(e). To further explore such microcavity without angular dispersion, we calculate the distributions of the magnetic field intensity enhancement $|H_y|/|H_0|$ ($H_0$ corresponds to the incidence) as a function of wavelength. The results for $\theta = 0°$ and $\theta = 80°$ are represented in Fig. 4(a) and (b), respectively. It is noted that compared with the field distribution at normal incidence, the resonant wavelength as well as the quality factor of the first-order microcavity resonance are almost kept the same at grazing incidence. The only distinction exists in the smaller field intensity, which is due to the larger reflection from air upon the metamaterials at grazing incidence.

Then we investigate the microcavity incorporating hyperbolic metamaterials with complex $\varepsilon_z$. The cavity parameters are still chosen as $n_c = 1.7$ and $d = 150$ nm. We define $\Delta\lambda$ as the resonant wavelength difference between $\theta = 80°$ and $\theta = 0°$, and approximately take $\Delta\lambda = 0$ as the criterion for a microcavity without angular dispersion. Fig. 5(a) displays the calculated $\Delta\lambda$ as a function of $\varepsilon_z$. The black line represents the region where $\Delta\lambda = 0$, from which we find the various choices of $\varepsilon_z$, not only on the negative real axis but also into the complex plane, to establish a microcavity without angular dispersion. However, the spectra with these values of
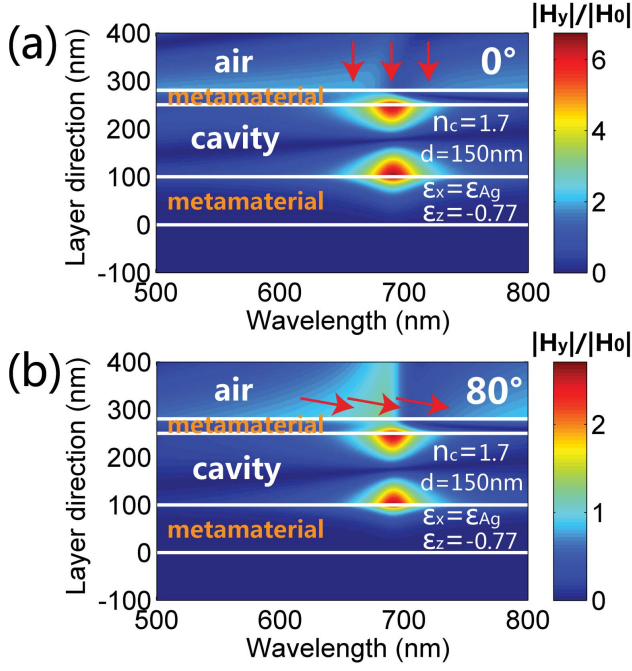
Fig. 4. Distributions of the magnetic field intensity enhancement in the microcavity without angular dispersion for TM-polarized incidence with $\theta = 0°$ (a) and $\theta = 80°$ (b).



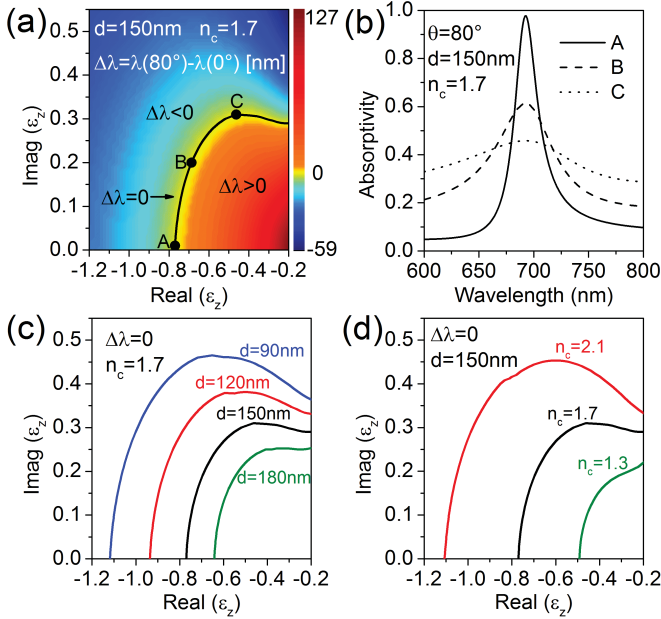Fig. 5. (a) Resonant wavelength difference $\Delta\lambda$ of the microcavity between $\theta = 80°$ and $\theta = 0°$ as a function of $\varepsilon_z$, where the black line represents the region where $\Delta\lambda = 0$. (b) TM-polarized absorptivity spectra at $\theta = 80°$ for three values of $\varepsilon_z$ marked as point A, B, and C in (a). (c)–(d) The calculated values of $\varepsilon_z$ for $\Delta\lambda = 0$ with different cavity thickness (c) and refractive index (d).

$\varepsilon_z$ exhibit distinctions. Fig. 5(b) shows the absorptivity spectra at $\theta = 80°$ for three values of $\varepsilon_z$ marked as point A, B, and C in Fig. 5(a). It is noted that the bandwidth of the microcavity resonance increases with $Im(\varepsilon_z)$. Therefore, in view of a large quality factor, one should choose $\varepsilon_z$ with an imaginary part as small as possible. Then we investigate the dependence of the

calculated values of $\varepsilon_z$ for $\Delta\lambda = 0$ on the cavity thickness and refractive index, with the results plotted in Fig. 5(c) and (d), respectively. In Fig. 5(c) where the cavity refractive index is fixed, we find that the calculated $\varepsilon_z$-line with a larger cavity thickness is closer to the original point. This is because that a thicker cavity will provide a larger decrement of $\varphi_{cavity}$ with the angle increasing, which should be compensated by a smaller $|\varepsilon_z|$ induced larger $\Delta\varphi_r$ (see (4)), and vice versa. In Fig. 5(d) where the cavity thickness is fixed, we know that a cavity with higher refractive index will provide a smaller decrement of $\varphi_{cavity}$ with the angle increasing, since

$$\varphi_{cavity}(\theta) - \varphi_{cavity}(0°) = -2k_0 d \sin^2\theta \Big/ \left(n_c + \sqrt{n_c^2 - \sin^2\theta}\right).$$

Therefore, to compensate such smaller phase decrement, a larger $|\varepsilon_z|$ induced smaller $\Delta\varphi_r$ is needed, and vice versa. This explains the trend that the calculated $\varepsilon_z$-line with a higher cavity refractive index is more far away from the original point.

### B. Realization of Microcavity Without Angular Dispersion

Finally, we demonstrate the possibility in realization of such microcavity by employing the realistic Ag-Ge multilayered structures [12], [14], [20] as the hyperbolic metamaterial reflectors. The potential structure is depicted in Fig. 6(a), in which the cavity parameters are chosen as $n_c = 1.7$, and $f_{Ag}$ ($= 0.7$) and $f_{Ge}$ ($= 0.3$) are the filling ratios of Ag and Ge, respectively. We assume the thickness of one Ag-Ge pair is far smaller than the operating wavelength. In such stacking direction, the effective permittivity can be solved based on the effective media theory [14] as $\varepsilon_x = \left(f_{Ag}/\varepsilon_{Ag} + f_{Ge}/\varepsilon_{Ge}\right)^{-1}$ and $\varepsilon_z = f_{Ag}\varepsilon_{Ag} + f_{Ge}\varepsilon_{Ge}$. The calculated $\varepsilon_x$ and $\varepsilon_z$ are plotted in Fig. 6(b) and (c), respectively, where we choose $\varepsilon_{Ge} = 4^2$. It is noted that in the wavelength range around 500 nm, the values of $\varepsilon_x$ much resemble those of metallic reflectors, with which the Ag-Ge multilayered structures can be guaranteed as reflectors for normal incidence. Besides, the real part of $\varepsilon_z$ is negative and near zero, while the imaginary part is also near zero. Therefore, the effective parameters of the Ag-Ge stack in this wavelength range may meet the requirements for the hyperbolic metamaterials discussed before. We then change the cavity thickness to tune the resonant wavelength. We find that with a cavity thickness of $d = 108$ nm, a microcavity without angular dispersion can be established at the wavelength of ~510 nm with constitutive parameters of $\varepsilon_x = -14.7 + 1.7j$ and $\varepsilon_z = -0.9 + 0.5j$, as shown by the dashed lines in Fig. 6(b) and (c). The TM-polarized absorptivity spectra are then calculated by the transfer matrix method based on these effective parameters and plotted in Fig. 6(d) for four incident angles, where the invariant resonant wavelength (~510 nm) with the angle increasing can be seen in the yellow region. The corresponding absorptivity dispersion is also illustrated in Fig. 6(e), where the features of the microcavity without angular dispersion can be intuitional seen from the blue dashed region. In this design strategy, the resonant wavelength of the microcavity can be tuned by changing the filling ratios of Ag and Ge in the multilayered structures.
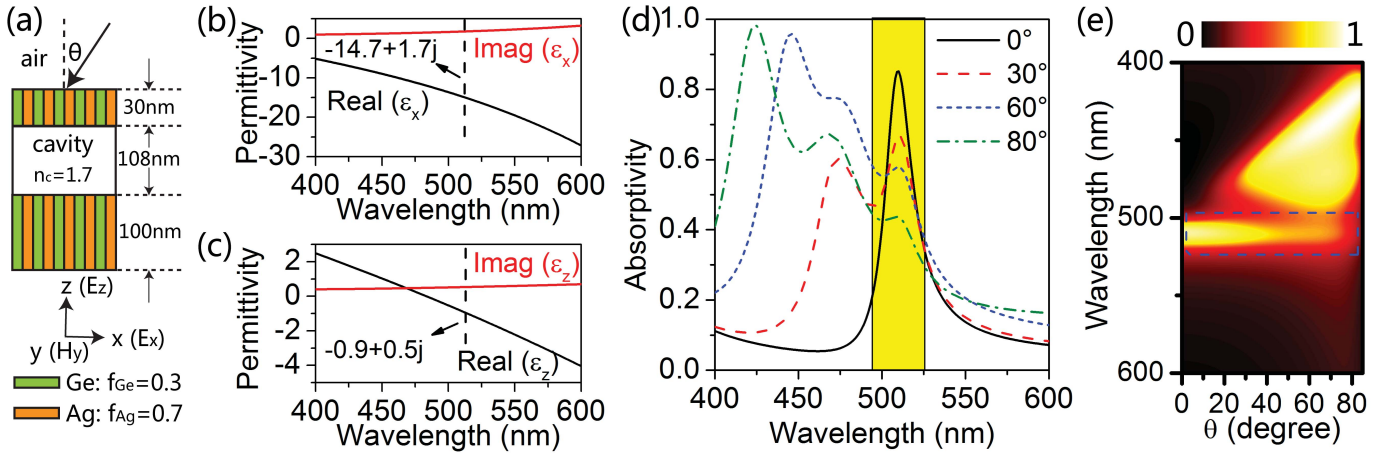
Fig. 6. (a) A potential realization of the microcavity by employing the realistic Ag-Ge multilayered structures as the hyperbolic metamaterials. (b)–(c) Calculated values of $\varepsilon_x$ (b) and $\varepsilon_z$ (c) based on the effective media theory. (d) TM-polarized absorptivity spectra of the structure in (a) for different incident angles. The yellow region indicates that the resonant wavelength is nearly invariant with the angle increasing. (e) Absorptivity dispersion of the microcavity as a function of wavelength and incident angle. The blue dashed region indicates the microcavity resonance without angular dispersion.

Although a microcavity without angular dispersion can be established by employing the Ag-Ge multilayered structures, unexpected resonant states emerge with the angle increasing, such as the resonant peaks located at ∼424 nm and ∼469 nm for the incident angle of 80°. To investigate such phenomenon, we calculate the phase variations for the incident angle of 0° and 80°, with the results shown in Fig. 7(a) and (b), respectively. It is noted that for the case of 0°, the variations of $\varphi_{up}$, $\varphi_{down}$, and $\varphi_{cavity}$ are all monotonous, resulting in only one intersection between $\varphi_{sum}$-line and $2\pi$-line. Therefore, only one microcavity resonance can be supported, as indicated by the black point in Fig. 7(a). For the case of 80°, the resonant wavelength of this microcavity resonance can be maintained via our design strategy, as verified by the black point in Fig. 7(b). However, the variations of $\varphi_{up}$ and $\varphi_{down}$ are no longer monotonous, which directly lead to multiple intersections between $\varphi_{sum}$-line and $2\pi$-line as well as additional microcavity resonances. Interestingly, all of these resonant states are first-order microcavity resonances, which can further be verified by the distributions of the magnetic field intensity enhancement in the structures. The results are illustrated in Fig. 7(c) and (d) for the incident angle of 0° and 80°, respectively, from which the designed invariant microcavity resonance at ∼510 nm as well as additional first-order resonances can be seen. Besides, in contrast with the designed microcavity resonance, the additional resonances exhibit strong dispersions with the angle increasing [Fig. 6(e)], which again shows the merit of our design. Moreover, the appearance of the multiple first-order resonances can be attributed to the non-monotonous reflection phases from the Ag-Ge multilayered structures, which are further induced by the strong dispersions of the permittivity [see Fig. 6(b) and (c)]. In our opinion, the appearance of the additional peaks with the angle increasing may be avoided by employing multilayered structures with weak dispersions, or by applying other types of metamaterials which exhibit our desired constitutive parameters.
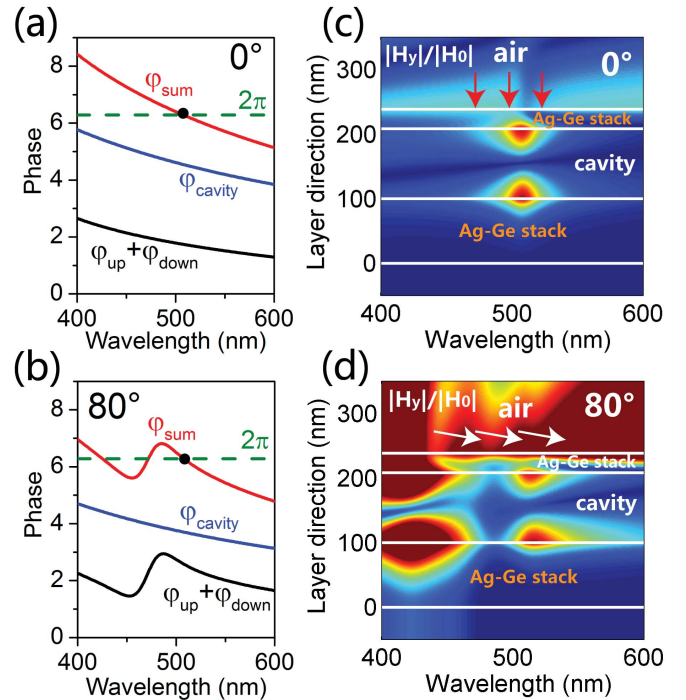


Fig. 7. Phase variations in the Ag-Ge multilayered structures based microcavity with incident angle of (a) 0° and (b) 80°. Distributions of the magnetic field intensity enhancement in the Ag-Ge multilayered structures based microcavity with incident angle of (c) 0° and (d) 80°. TM-polarized incidence is applied in all these calculations.

## III. CONCLUSION

To conclude, we have established a microcavity without angular dispersion by employing metamaterials with hyperbolic dispersion as the reflectors. In such a microcavity, the reflection phase from the cavity upon the metamaterial reflectors exhibits a drastic increment with the angle increasing, which can, for each incident angle, nearly compensate the decrement of the phase accumulation inside the cavity.

Based on this design principle, a microcavity exhibiting a red shift of the resonance with the angle increasing can even be designed. In practice, such hyperbolic metamaterials may be realized by employing the metal-dielectric multilayered structures. Besides, as other works employing the hyperbolic metamaterials [14], [20], the design in our work also only applies to one polarization-TM polarization, whereas a design for TE polarization may require metamaterials with exotic magnetic response.

## REFERENCES

[1] B. Yu, A. Wang, and G. R. Pickrell, "Analysis of fiber Fabry–Pérot interferometric sensors using low-coherence light sources," *J. Lightw. Technol.*, vol. 24, no. 4, pp. 1758–1767, Apr. 2006.

[2] C. Y. Lu, S. L. Chuang, and D. Bimberg, "Metal-cavity surface-emitting nanolasers," *IEEE J. Quantum Electron.*, vol. 49, no. 1, pp. 114–121, Jan. 2013.

[3] J. Masson, R. S. Gelais, A. Poulin, and Y. A. Peter, "Tunable fiber laser using a MEMS-based in plane Fabry–Pérot filter," *IEEE J. Quantum Electron.*, vol. 46, no. 9, pp. 1313–1319, Sep. 2010.

[4] C. Xiang, W. Koo, F. So, H. Sasabe, and J. Kido, "A systematic study on efficiency enhancements in phosphorescent green, red and blue microcavity organic light emitting devices," *Light, Sci. Appl.*, vol. 2, p. e74, Jun. 2013.

[5] Y. F. Liu et al., "Omnidirectional emission from top-emitting organic light-emitting devices with microstructured cavity," *Opt. Lett.*, vol. 37, no. 2, pp. 124–126, Jan. 2012.

[6] Y. F. Liu et al., "Viewing-angle independence of white emission from microcavity top-emitting organic light-emitting devices with periodically and gradually changed cavity length," *Org. Electron.*, vol. 14, no. 6, pp. 1597–1601, Jun. 2013.

[7] Y. Jin et al., "Solving efficiency-stability tradeoff in top-emitting organic light-emitting devices by employing periodically corrugated metallic cathode," *Adv. Mater.*, vol. 24, no. 9, pp. 1187–1191, Mar. 2012.

[8] X. L. Zhang, J. F. Song, X. B. Li, J. Feng, and H. B. Sun, "Light trapping schemes in organic solar cells: A comparison between optical Tamm states and Fabry–Pérot cavity modes," *Org. Electron.*, vol. 14, no. 6, pp. 1577–1585, Jun. 2013.

[9] N. Tessler, S. Burns, H. Becker, and R. H. Friend, "Suppressed angular color dispersion in planar microcavities," *Appl. Phys. Lett.*, vol. 70, no. 5, pp. 556–558, Jun. 2009.

[10] A. B. Djurišic and A. D. Rakic, "Asymmetric Bragg mirrors for the reduction of emission wavelength dependence on the viewing angle in organic microcavity light emitting diodes," *Opt. Commun.*, vol. 236, nos. 4–6, pp. 303–311, Jun. 2004.

[11] W. C. H. Choy and C. Y. Ho, "Improving the viewing angle properties of microcavity OLEDs by using dispersive gratings," *Opt. Exp.*, vol. 15, no. 20, pp. 13288–13294, Oct. 2007.

[12] X. Yang, J. Yao, J. Rho, X. Yin, and X. Zhang, "Experimental realization of three-dimensional indefinite cavities at the nanoscale with anomalous scaling laws," *Nature Photon.*, vol. 6, no. 7, pp. 450–454, Jun. 2012.

[13] B. Zhang, "Electrodynamics of transformation-based invisibility cloaking," *Light, Sci. Appl.*, vol. 1, p. e32, Oct. 2012.

[14] L. Sun, S. Feng, and X. Yang, "Loss enhanced transmission and collimation in anisotropic epsilon-near-zero metamaterials," *Appl. Phys. Lett.*, vol. 101, no. 24, pp. 241101-1–241101-4, Dec. 2012.

[15] P. Dardano, M. Gagliardi, I. Rendina, S. Cabrini, and V. Mocella, "Ellipsometric determination of permittivity in a negative index photonic crystal metamaterial," *Light, Sci. Appl.*, vol. 1, p. e42, Dec. 2012.

[16] N. Papasimakis, S. Thongrattanasiri, N. I. Zheludev, and F. G. Abajo, "The magnetic response of grapheme split-ring metamaterials," *Light, Sci. Appl.*, vol. 2, p. e78, Jul. 2013.

[17] M. Born and E. Wolf, *Principles of Optics*. Cambridge, U.K.: Cambridge Univ. Press, 2003.

[18] P. Yeh, *Optical Waves in Layered Media*. New York, NY, USA: Wiley, 1988.

[19] P. B. Johnson and R. W. Christy, "Optical constants of the noble metals," *Phys. Rev. B*, vol. 6, no. 12, pp. 4370–4379, Dec. 1972.

[20] L. Sun, J. Gao, and X. Yang, "Broadband epsilon-near-zero metamaterials with steplike metal-dielectric multilayer structures," *Phys. Rev. B*, vol. 87, no. 16, pp. 165134-1–165134-6, Apr. 2013.
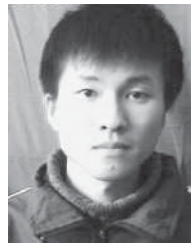
**Xu-Lin Zhang** received the B.S. degree in electronic information and science technology from the College of Electronic Science and Engineering, Jilin University, China, in 2009, where he is currently pursuing the Ph.D. degree. His current research interests include metamaterials-based optoelectronics devices.

**Jun-Feng Song** received the B.S. and Ph.D. degrees from the College of Electronic Science and Engineering, Jilin University, China, in 1993 and 2000, respectively. He was a Post-Doctoral Researcher with the Changchun Institute of Optics, Chinese Academy of Sciences, from 2000 to 2002. He is currently a Professor with Jilin University. His current research interests include silicon-based optics devices, photonic crystal fibers, and wavelength shifters.

**Jing Feng** received the B.S. and Ph.D. degrees from the College of Electronic Science and Engineering, Jilin University, China, in 1997 and 2003, respectively. She was a Post-Doctoral Researcher at RIKEN, Japan, from 2003 to 2006, and is currently a Professor with Jilin University. Her current research interests include organic optoelectronics and optoelectronic devices.

**Hong-Bo Sun** received the B.S. and Ph.D. degrees in optoelectronics from Jilin University, China, in 1992 and 1996, respectively. He was a Post-Doctoral Researcher with the University of Tokushima, Japan, from 1996 to 2000, and then as an Assistant Professor with the Department of Applied Physics, Osaka University, Osaka, Japan. In 2005, he was promoted to Full professor (Changjiang Scholar Professor) in Jilin University. His research interests have been laser nanofabrication and ultrafast spectroscopy: fabrication of various microoptical, microelectronical, micromechanical, microoptoelectronic, microfluidic components and integrated systems at nanoscales, and exploring ultrafast dynamics of photons, electrons, phonons, and surface plasmons in solar cells, organic light-emitting devices, and low-dimensional quantum systems at femtosecond timescale. He has authored more than 200 scientific papers and delivered more than 150 invited talks at international conferences. The total SCI citations to his papers are around 6000 times. He also served as the General/Technical Co-Chairs of a large number of conferences.